These results suggest a mechanism of signaling conserved between BRI1 and XA21 that may be extrapolated to the large number of LRR-RLKs found in plant genomes. The model would include ligand perception through the extracellular/transmembrane domain, whereas the intracellular kinase domain determines the downstream signaling response. There are greater than 120 LRR-RLKs predicted in the *Arabidopsis* genome sequencing project. The chimeric receptor approach, using the XA21 signaling outputs defined here, should provide an assay system that is applicable to the discovery of ligands for the LRR-RLKs, as well as aid in the design of novel signaling genes for controlling plant development and disease resistance.

References and Notes

1. P. van der Geer, T. Hunter, R. Lindberg, *Annu. Rev. Cell Biol.* **10**, 251 (1994).
2. J. Massagué, *Cell* **85**, 947 (1996).
3. X. Feng and R. Deryneck, *EMBO J.* **16**, 3912 (1997).
4. K. Lease, E. Ingham, J. C. Walker, *Curr. Opin. Plant Biol.* **1**, 388 (1998).
5. P. Becraft, *Trends Plant Sci.* **3**, 384 (1998).
6. S. Clark, R. Williams, E. Meyerowitz, *Cell* **89**, 575 (1997).
7. W. Song *et al.*, *Science* **270**, 1804 (1995).
8. J. Li and J. Chory, *Cell* **90**, 92 (1997).
9. K. Torii *et al.*, *Plant Cell* **8**, 735 (1996).
10. T. L. Lin, J. Stone, J. Walker, *Genes Dev.* **14**, 108 (2000).
11. J. Fletcher, U. Brand, M. Running, R. Simon, E. Meyerowitz, *Science* **283**, 1911 (1999).
12. G. Martin, *Curr. Opin. Plant Biol.* **2**, 273 (1999).
13. A. Levine, R. Tenhaken, R. Dixon, C. Lamb, *Cell* **79**, 583 (1994).
14. Rice transformation was as described [L. Chen, S. Zhang, R. N. Beachy, C. M. Fauquet, *Plant Cell Rep.* **18**, 25 (1998)]. Cell suspension lines were established in NB6 medium from transformants. The XA21 cell line was established from homozygous seeds of XA21 transgenic line 106 (7).
15. Z. He and P. Ronald, unpublished data.
16. Q. Zhu and C. Lamb, *Mol. Gen. Genet.* **226**, 289 (1991).
17. Q. Zhu *et al.*, *Plant Mol. Biol.* **29**, 535 (1995).
18. M. Yoshikawa and P. Ronald, unpublished data.
19. W. Song and P. Ronald, unpublished data.
20. S. Yi, S. Yu, D. Choi, *Mol. Cell* **9**, 320 (1999).
21. J. Li, P. Nagpal, V. Vitart, T. C. McMorris, J. Chory, *Science* **272**, 398 (1996).
22. D. Friedrichsen, C. Joazeiro, J. Li, T. Hunter, J. Chory, *Plant Physiol.*, in press.
23. After treatment, media were filtered to remove cells with 0.2-μm syringe filters. One hundred–microliter samples were added to 1 ml of reaction buffer [0.25 mM $FeSO_4$, 0.25 mM $(NH_4)_2SO_4$, 25 mM H_2SO_4, 1.25 μM xylenol orange, and 1 mM sorbitol] at room temperature for 1 hour. Absorbance was measured at 560 nm, and H_2O_2 levels were calculated by reference to standards [Z. Jiang, J. V. Hunt, S. P. Wolff, *Anal. Biochem.* **202**, 383 (1992)].
24. RNA was extracted from the XA21 cell lines at 0 to 24 hours after inoculation with P6 and K1 (10^7 cells per milliliter), with the TRIzol reagent (Life Technologies, Gaithersburg, MD). Thirty micrograms of total RNA was used in each lane. A 1.2-kb fragment of rice chitinase *RCH10* (13), a 400–base pair fragment of *PAL* (17), and a cDNA clone of *OsCatB* (19) were used as probes. The filters were reprobed with 18*S Arabidopsis* rDNA for normalization.
25. A *BRI1* DNA fragment encoding the presumed extracellular, transmembrane (TM), and juxtamembrane (JM) domains [amino acids 1 to 879 (8)] was fused with the *Xa21* fragment encoding the predicted kinase domain [amino acids 708 to 1025 (7)] to make NRG1. NRG2 consisted of amino acids 1 to 769 of BRI1 and the XA21 TM, JM, and kinase domains with amino acids 625 to 1025. NRG3 consisted of amino acids 1 to 834 of BRI1 and amino acids 684 to 1025 of XA21. NRG1mL contains a mutation (Gly^{611} → Glu) corresponding to the allele *bri1-113* (8). NRG1mK is a mutation of XA21 (Lys^{737} → Glu) obtained by in vitro mutagenesis with the primer (5′-GTTGCAGTGGAGGTACTAA-3′) corresponding to the *Xa21* sequence 2197 to 2215 (7).
26. Cells were homogenized in 50 mM tris-HCl (pH 7.5), 200 mM mannitol, 10 mM $MgCl_2$, and protease inhibitor cocktail (Boehringer Mannheim). After centrifugation at 10,000*g* for 20 min, the supernatant was centrifuged at 100,000*g* for 1 hour to collect membranes. Membrane proteins (80 μg per lane) were resolved on a 3 to 8% gradient SDS-NuPAGE gel (Invitrogen), transferred to nitrocellulose, and probed with affinity-purified antibodies raised to BRI1's NH_2-terminal 106 amino acids.

27. We thank S. Zhang and L. Chen for providing facilities for biolistic bombardment; L. Klimczak for bioinformatics guidance; T. Murphy for the H_2O_2 protocol; R. Ruan and T. Dabi for cell line maintenance; Y. Shen for technical help; and R. Larkin, D. Weigel, Y. Yin, and Y. Zhao for helpful comments on the manuscript. This work was supported by grants from the U.S. Department of Agriculture to J.C. and C.L., from NIH to P.R., and the Rockefeller Foundation International Program on Rice Biotechnology (Z.H., P.R., and C.L.). Z.W. is an NSF postdoctoral fellow and J.C. is an Associate Investigator of the Howard Hughes Medical Institute.

22 March 2000; accepted 4 May 2000

Perception of Environmental Signals by a Marine Diatom

Angela Falciatore,[1] Maurizio Ribera d'Alcalà,[2] Peter Croot,[3] Chris Bowler[1]*

Diatoms are a key component of marine ecosystems and are extremely important for the biogeochemical cycling of silica and as contributors to global fixed carbon. However, the answers to fundamental questions such as what diatoms can sense in their environment, how they respond to external signals, and what factors control their life strategies are largely unknown. We generated transgenic diatom cells containing the calcium-sensitive photoprotein aequorin to determine whether changes in calcium homeostasis are used to respond to relevant environmental stimuli. Our results reveal sensing systems for detecting and responding to fluid motion (shear stress), osmotic stress, and iron, a key nutrient that controls diatom abundance in the ocean.

The predominance of diatoms in marine ecosystems indicates that they possess sophisticated strategies for responding to environmental variation. However, little is known about these strategies at the cellular level because of the difficulties of monitoring key internal physiological processes in these organisms. The recent availability of procedures to generate transgenic diatoms (*1–3*) has opened up a range of techniques that can be used to address these questions.

We transformed the marine diatom *Phaeodactylum tricornutum* (*4*) with a construct containing the apoaequorin cDNA derived from the jellyfish *Aequorea victoria* (*5*). Transgenic cells displaying high levels of aequorin were selected (*4*) and used to analyze diatom responses to a range of different stimuli.

Transient changes in cytosolic calcium concentrations ($[Ca^{2+}]_{cyt}$), which are characteristic of the activation of signal transduction (*6*), could be observed in response to the simple addition of seawater [artificial seawater (ASW)] (Fig. 1A). A maximal increase in $[Ca^{2+}]_{cyt}$ from 500 nM to 2 μM was observed after 1 to 2 s, which quickly disappeared within 10 s. This response weakened with declining stimulus strength (*7*). To exclude the possibility that chemical signaling may have been involved as a result of the addition of fresh medium to the cells, we confirmed that conditioned medium (medium in which the diatoms had been growing) was able to generate the same effects, as was the mechanical stimulation of the cell suspension with a needle (Fig. 1A). When these experiments were repeated with a pH microelectrode in the suspension, no changes in pH were detected after the treatments (*8*), thus excluding the possibility that the observed calcium responses were a consequence of external pH changes.

When organisms are exposed to a stimulus for a long enough period, they typically lose their ability to respond with their original sensitivity. By this process of short-term adaptation or desensitization, a cell reversibly adjusts its sensitivity to the level of the stimulus. At the molecular level, the best understood examples of adaptation occur in bacterial chemotaxis (*9*) and in photoperception in the retina (*10*). To determine whether diatoms possess such sophisticated sensing systems for responding to fluid motion, we examined the effect of giving

[1]Laboratories of Molecular Plant Biology and [2]Biological Oceanography, Stazione Zoologica Anton Dohrn, Villa Comunale, I-80121 Naples, Italy. [3]Department of Marine Chemistry and Geology, Netherlands Institute for Sea Research (NIOZ), Postbus 59, 1790 AB Den Burg, Texel, Netherlands.

*To whom correspondence should be addressed. E-mail chris@alpha.szn.it

two successive stimuli to the same cells (Fig. 1B). If a second treatment immediately followed the initial stimulus (for example, after 5 s), no difference in the response was observed. However, when the time between the two treatments was increased (from 30 s to 5 min), the response was desensitized (Fig. 1B). This "recalcitrant period" lasted for approximately 5 min before the cells became progressively resensitized once more (after 10 to 15 min). The response to fluid motion is therefore rapid (seconds) and highly controlled, and the time scale for intracellular adjustments to changes in the cell boundary layer appears to be on the order of minutes. Furthermore, the observation that diatom desensitization develops slowly (up to 5 min) is unlike typical desensitization processes in higher eukaryotes, where no response is commonly observed if the second stimulus is applied shortly after the first.

We also analyzed diatom responses to osmotic stress. Many organisms, such as bacteria and plants, have evolved mechanisms to adjust their internal osmolarity in response to osmotic stress, based on the intracellular accumulation of ions or other osmolytes (*11, 12*). Diatoms were given a hypo-osmotic stress by treatment of ASW-grown cells with diluted ASW (Fig. 2A). Again, the $[Ca^{2+}]_{cyt}$ response was rapid and transient, and reflected quantitatively the amount of stress imposed on the cells (Fig. 2B). In general, the response was stronger than the shear response [for example, the $[Ca^{2+}]_{cyt}$ peak was around 4 μM in 80% ASW (Fig. 2A)]. To determine whether this response was due to an osmotic response or to the dilution of a particular ion, diatoms were incubated in a sucrose solution with an osmolarity equivalent to that of 100% ASW (Fig. 2C). Reductions in osmolarity by dilution of sucrose were found to provoke responses identical to those seen with dilution of ASW, thus confirming that this response was due to an osmotic sensing mechanism. The possibility that the responses to hypo-osmotic stress were an artefact of cell lysis was excluded by determining diatom uptake of Evans blue (*13*).

We tested desensitization to hypo-osmotic shock by performing two treatments separated by different time intervals. In contrast to shear, no desensitization was observed in response to hypo-osmotic shock (Fig. 2D). This result therefore indicated substantial differences between the signal transduction pathways for the two different stimuli, which could correspond to distortion and dilution, respectively, of the cell boundary layer.

Although reductions in osmolarity yielded a quantitatively appropriate response that was proportional to the reduction, a hyper-osmotic shock produced no change in cytosolic calcium above the shear signal (Fig. 2B). However, it was possible to adapt the cells to a particular osmolarity (for example, 1140 mosmol), and the response to a reduction of 100 mosmol was identical to that observed in cells adapted to 940 mosmol and then shifted to 840 mosmol (*14*). Tidal diatoms are likely to be exposed regularly to both hypo- and hyper-osmotic shocks, so one might suppose that a different sensing mechanism (one that does not rely on calcium) is used to detect and quantify hyper-osmotic conditions.

In contrast with higher plant cells (*15, 16*), alterations in temperature did not result in any changes in $[Ca^{2+}]_{cyt}$ above the basal shear response (Fig. 2A). This may reflect a divergent importance of temperature changes between terrestrial and marine ecosystems; that is, temperature variability on land exhibits a much greater range and more rapid variability than in the ocean.

External nutrient concentrations are key regulators of phytoplankton growth. In the marine environment, nutrients such as nitrate, silicate, and phosphate are extremely important, and strong evidence also implicates dissolved iron as being a limiting resource for phytoplankton growth, particularly in high-nutrient, low-chlorophyll (HNLC) regions of

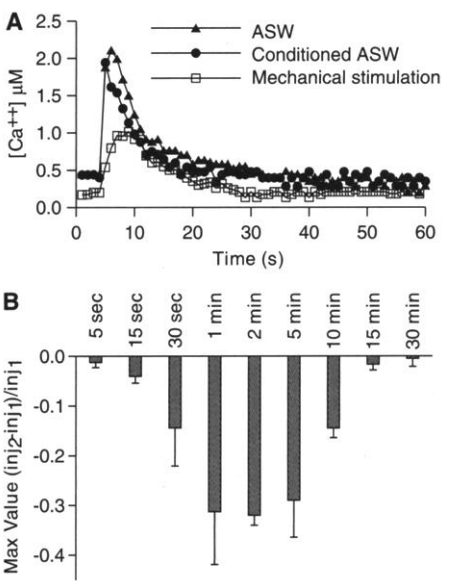

Fig. 1. Influence of fluid motion on cytosolic calcium. (**A**) Approximately 10^4 cells suspended in 50 μl of ASW were stimulated by the addition of 50 μl of fresh medium (ASW) or conditioned medium, or by mechanical stimulation performed with a needle. Treatments were performed 3 s after the beginning of the trace. (**B**) Adaptive responses to shear. Cells (10^4 in 50 μl of fresh medium) were given two successive stimuli of the same intensity. Times between the two stimuli were 5 s, 15 s, 30 s, 1 min, 2 min, 5 min, 10 min, 15 min, and 30 min. The graph shows the differences between the maximal $[Ca^{2+}]_{cyt}$ obtained with the second treatment (inj_2) with respect to the $[Ca^{2+}]_{cyt}$ in response to the first stimulus (inj_1), normalized with respect to the first response $[(inj_2 - inj_1)/inj_1]$. Standard deviations are shown (n = 5 repetitions).

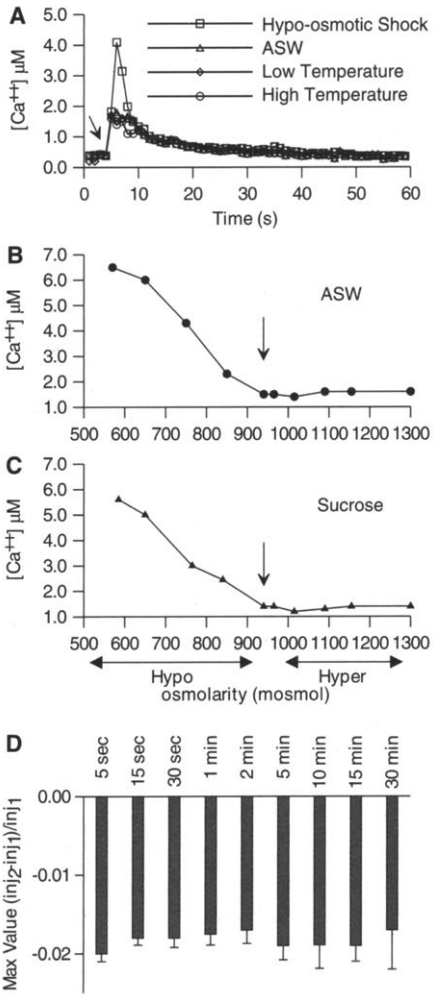

Fig. 2. Influence of osmotic stress. (**A**) Diatom responses to hypo-osmotic shock, fluid motion, and low- and high-temperature treatments. Diatom cells (10^4) in 100 μl of fresh medium (100% ASW) were stimulated with 25 μl of distilled water to generate a hypo-osmotic shock (80% ASW final); cells were also stimulated with ice-cold and warm (37°C) media. (**B**) Effect of osmolarity differences on hypo-osmotic shock–induced cytosolic Ca^{2+} elevations. Osmotic shocks were generated by injecting 50 μl of different dilutions of fresh media (ASW) to 10^4 cells in 100% ASW. (**C**) The same osmolarity differences were also generated by injection of different concentrations of sucrose solutions to the cells suspended in a sucrose solution with an osmolarity equivalent to that of 100% seawater. Arrows show the osmolarity of 100% ASW and in the corresponding sucrose solution (940 mosmol). The osmotic pressure of solutions was measured with a micro-osmometer (Roebling). (**D**) Diatom cells in 100 μl of fresh medium were stimulated by two successive treatments of distilled water that generated the same hypo-osmotic shock (80% ASW, final salt concentration). Times between the two stimuli were 5 s, 15 s, 30 s, 1 min, 2 min, 5 min, 10 min, 15 min, and 30 min. The graph shows the differences between $[Ca^{2+}]_{cyt}$ peaks obtained with the second treatment (inj_2) with respect to the $[Ca^{2+}]_{cyt}$ in response to the first stimulus (inj_1), normalized with respect to the first response $[(inj_2 - inj_1)/inj_1]$. Standard deviations are shown (n = 5 repetitions).

the contemporary ocean (*17*, *18*). The "iron hypothesis" has recently been tested and supported, at least for short time scales, through mesoscale iron fertilization experiments in HNLC regions (*19*, *20*). Consequently, new methods have been developed to determine iron deficiency in phytoplankton, such as the analysis of photochemical quantum efficiency based on variable fluorescence measurements (*21*) and the use of immunological probes (*22*, *23*).

We measured $[Ca^{2+}]_{cyt}$ changes in response to varying nutrient concentrations. No changes in cytoplasmic calcium in response to nitrate, nitrite, ammonium, silicate, or phosphate were observed in either nutrient-replete (Fig. 3) or depleted (*8*) conditions. However, a response to dissolved iron was detected (Fig. 3), and in this case the calcium signature was very different from that observed after shear or hypo-osmotic shock: the response was not evident until about 5 min after iron addition, and $[Ca^{2+}]_{cyt}$ continued to rise for a considerable time afterward. This time course closely resembles that of iron internalization rates in diatoms (*24*), although it is not possible in these experiments to know whether calcium has a direct effect on iron uptake. However, aequorin has no specific affinity for Fe^{2+} and Fe^{3+} (*25*), thus excluding the possibility that the observed bioluminescence was an artefact due to iron-stimulated aequorin light emission.

We grew diatoms in ASW containing iron concentrations ranging from 10 nM to 10 μM (*26*). In 10 nM $FeCl_3$, cells were clearly growth-limited (Fig. 4A) and in response to the addition of 20 to 30 pM dissolved inorganic iron (Fe′) only these cells showed a response, which was slow and weak (Fig. 4B). However, after the addition of a larger amount of iron (Fe′ = 48 to 60 pM), cells from all cultures responded, and it was possible to observe differences in the timing and kinetics of the responses (Fig. 4C). These results indicate that diatoms control iron metabolism using calcium-mediated regulatory mechanisms and that one component of this regulation prevents iron assimilation at very low concentrations unless the cell is extremely starved. Less starved cells, on the other hand, activate iron uptake only at higher iron concentrations. Therefore, the relationship between bioavailable iron and cellular response is not linear but depends on the history and physiology of the cells. The complex kinetics shown in Fig. 4 and the differences in response between the most iron-starved culture and the other three cultures may indicate that in the iron-starved case, the available iron had been completely exhausted from the solution [consistent with the growth rate and iron demand of this culture (Fig. 4A)] and that all the ligand sites on the cell membrane were free of iron. If so, our results suggest a thermodynamic rather than a kinetic control of iron uptake (*27*). Measurement of the calcium response could therefore be a very sensitive tool for kinetic studies and, more important, a good marker for iron starvation, because the dramatic changes observed may represent intracellular signals for the reactivation of cell division, the stimulation of photosynthesis, and the activation of mitochondrial ATP (adenosine triphosphate) production that are known to occur under conditions of favorable iron bioavailability (*21*, *28*).

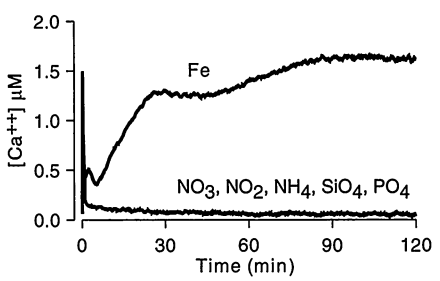

Fig. 3. Diatom responses to nutrients. $[Ca^{2+}]_{cyt}$ elevations in response to the addition of different nutrients are shown. 10^4 cells in 50 μl of ASW were treated with enriched ASW containing 1 mM $NaNO_3$, 1 mM $NaNO_2$, 1 mM NH_4Cl, 1 mM Na_2SiO_3, 1 mM NaH_2PO_4, or 10 μM $FeCl_3$. The initial calcium spike seen in all the traces corresponds to the fluid motion response.

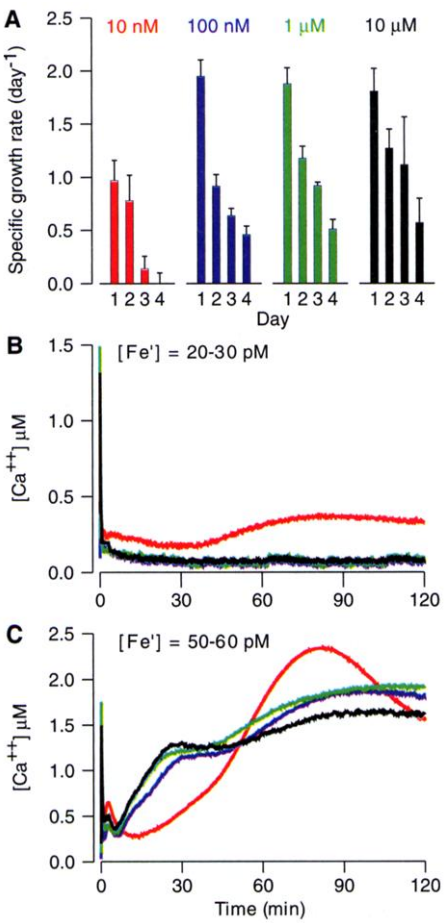

Fig. 4. $[Ca^{2+}]_{cyt}$ changes in response to $FeCl_3$ addition. (**A**) Specific growth rate (per day) of cells grown in ASW containing the iron concentrations indicated at the top of the panel (*26*). Experiments were performed at day 4, when the cells containing 10 nM $FeCl_3$ were clearly iron-limited. Before the addition of iron, cells were washed twice in ASW without $FeCl_3$ to remove all detectable traces of iron and were subsequently treated with enriched ASW containing 5 μM $FeCl_3$ (**B**) and 10 μM $FeCl_3$ (**C**), respectively. The dissolved inorganic iron contents (Fe′) of the growth media after these additions are shown.

The historical paradigm that plankton are passive and incapable of resisting physical forces at any scale (*29*) has already been superseded by evidence for the existence of active responses controlling buoyancy, local fluid viscosity, and life cycle (*30*–*32*). Our data indicate that diatoms detect and respond to physicochemical changes in their environment using sophisticated perception systems based on changes in $[Ca^{2+}]_{cyt}$. Such processes are likely to improve algal adaptation to ubiquitous ocean processes such as mixing and to changes in chemical (for example, nutrient) gradients in time and space. Based on the knowledge of calcium signaling in other organisms, the physiological responses of diatoms to environmental changes are likely to be regulated by sense-process-respond chains involving specific receptors and feedback mechanisms, whose activity is determined by the previous history of the cell. Therefore, the frequent assumption (especially in modeling efforts) that physiological responses of phytoplankton vary monotonically with resource availability is not correct. This new perspective should be considered in future studies and simulations of plankton dynamics.

References and Notes

1. T. G. Dunahay, E. E. Jarvis, P. G. Roessler, *J. Phycol.* **31**, 1004 (1995).
2. K. E. Apt, P. G. Kroth-Pancic, A. R. Grossman, *Mol. Gen. Genet.* **252**, 572 (1996).
3. A. Falciatore, R. Casotti, C. Leblanc, C. Abrescia, C. Bowler, *Mar. Biotech.* **1**, 239 (1999).
4. For further details, see *Science* Online at www.sciencemag.org/feature/data/1048586.shl.
5. M. Brini *et al.*, *J. Biol. Chem.* **270**, 9896 (1995).
6. D. E. Clapham, *Cell* **80**, 259 (1995).
7. For further details, see Web fig. 1 at (*4*).
8. A. Falciatore, M. Ribera d'Alcalà, P. Croot, C. Bowler, data not shown.
9. D. E. Koshland, *Annu. Rev. Biochem.* **50**, 765 (1981).
10. L. Stryer, *Proc. Natl. Acad. Sci. U.S.A.* **93**, 557 (1996).
11. L. N. Csonka and A. D. Hanson, *Annu. Rev. Microbiol.* **45**, 569 (1991).
12. D. Le Rudulier, A. R. Strom, A. M. Dandekar, L. T. Smith, R. C. Valentine, *Science* **224**, 1064 (1984).
13. Samples were incubated for 10 min with 0.05% Evans blue (Sigma) and then washed extensively to remove excess and unbound dye. Dye bound to dead cells was solubilized in 50% methanol with 1% sodium dodecyl sulfate for 20 min at 50°C and quantified by absorbance at 600 nm. Under the osmotic conditions tested in Fig. 2, no cell death could be detected.
14. For further details, see Web fig. 2 at (*4*).
15. H. Knight, A. J. Trewavas, M. R. Knight, *Plant Cell* **8**, 489 (1996).
16. C. Plieth, U. Hansen, H. Knight, M. R. Knight, *Plant J.* **18**, 491 (1999).
17. J. H. Martin and R. M. Gordon, *Deep-Sea Res.* **35**, 177 (1988).
18. J. H. Martin, R. M. Gordon, S. E. Fitzwater, *Nature* **345**, 156 (1990).

19. J. H. Martin *et al.*, *Nature* **371**, 123 (1994).
20. K. H. Coale *et al.*, *Nature* **383**, 495 (1996).
21. M. J. Behrenfeld and Z. S. Kolber, *Science* **283**, 840 (1999).
22. J. LaRoche, H. Murray, M. Orellana, J. Newton, *J. Phycol.* **31**, 520 (1995).
23. J. LaRoche, P. W. Boyd, R. M. L. McKay, R. J. Geider, *Nature* **382**, 802 (1996).
24. R. J. M. Hudson and F. M. M. Morel, *Limnol. Oceanogr.* **35**, 1002 (1990).
25. O. Shimomura and H. J. Frank, *Biochem. Biophys. Res. Commun.* **53**, 490 (1973).
26. Iron was provided as ferric chloride ($FeCl_3$) and added at final concentrations of 10 nM, 100 nM, 1 μM, and 10 μM. All the polycarbonate containers used to make ASW and to store the stock solutions were precleaned with 10% HCL-Milli Q water (1-week treatment) and subsequently washed with Milli Q water. All solutions were prepared in Milli Q water. Iron limitation was achieved by transfer of an exponentially growing culture (5 ml) initially containing 10 μM $FeCl_3$ (normal ASW concentrations) into 100 ml of ASW medium containing 0.1 mM EDTA with different iron concentrations (10 nM, 100 nM, 1 μM, and 10 μM $FeCl_3$). Experiments were performed only after a late-log-phase culture had passed through at least five successive rounds of growth for 7 days each under different iron-starvation media conditions. All experiments were repeated five times. The amount of dissolved iron (0.2 μm filtered) was determined with graphite furnace atomic absorption spectrophotometry. Measurements of Fe′ were made by means of adsorptive cathodic stripping voltammetry with 2-(2-thiazolylazo)-p-cresol [P. A. M. Farias *et al.*, *Anal. Lett.* **25**, 1929 (1992)].
27. R. J. M. Hudson and F. M. M. Morel, *Limnol. Oceanogr.* **40**, 129 (1993).
28. R. M. L. McKay, R. J. Geider, J. LaRoche, *Plant Physiol.* **114**, 615 (1997).
29. H. U. Sverdrup, M. W. Johnson, R. H. Fleming, in *The Oceans* (Prentice-Hall, New York, 1942), p. 281.
30. T. A. Villareal *et al.*, *Nature* **397**, 423 (1999).
31. I. R. Jenkinson, *Nature* **323**, 435 (1986).
32. H. C. H. R. Eilertsen, S. Sandberg, H. Tollefsen, *Mar. Ecol. Prog. Ser.* **116**, 303 (1995).
33. We thank R. Rizzuto, P. Pinton, J. Alvarez, and G. Neuhaus for advice on calcium calibration; L. Navazio and M. Brini for assistance with the mechanical stimulation experiments; B. van der Wagt (NIOZ) for help with the iron measurements; and T. Wyatt, I. Jenkinson, and C. Brownlee for critical reading of the manuscript. This paper is dedicated to the memory of Professor Gaetano Salvatore.

12 January 2000; accepted 2 May 2000

Cholinergic Synaptic Inhibition of Inner Hair Cells in the Neonatal Mammalian Cochlea

Elisabeth Glowatzki* and Paul A. Fuchs

Efferent feedback onto sensory organs provides a means to modulate input to the central nervous system. In the developing mammalian cochlea, inner hair cells are transiently innervated by efferent fibers, even before sensory function begins. Here, we show that neonatal inner hair cells are inhibited by cholinergic synaptic input before the onset of hearing. The synaptic currents, as well as the inner hair cell's response to acetylcholine, are mediated by a nicotinic (α9-containing) receptor and result in the activation of small-conductance calcium-dependent potassium channels.

In the mature mammalian cochlea, inner hair cells (IHCs) transduce acoustic signals into receptor potentials and communicate to the brain by synaptic contact with as many as 20 unbranched afferent fibers (*1*). In contrast, outer hair cells (OHCs) have few afferent contacts but are the principal target of cholinergic olivocochlear efferents. However, before the onset of hearing [about postnatal day 11 in rats (*2*)], a transient efferent innervation is found on IHCs, even before olivocochlear fibers contact the OHCs. These transient contacts have been documented in several species (*3*), suggesting that at least some of this innervation might be cholinergic; however, these synapses have never been shown to be functional nor have IHCs been shown to be sensitive to acetylcholine (ACh).

We used whole-cell recording of IHCs in acutely excised apical turns of the rat organ of Corti (postnatal days 7 to 13) (*4*) to examine the functional role of the transient synaptic contacts on immature IHCs. Because efferent axons are cut in this preparation, we relied on spontaneous transmitter release. Spontaneous transient currents were observed in 57 rat IHCs (~50% of IHCs tested) (Fig. 1). These occurred at rates of 0.5 per minute up to 15 per second and persisted for up to 10 min. At −80 mV, the spontaneous currents were inward with an amplitude of 16 ± 4 pA, rose rapidly (time to peak, 5 ± 2 ms), and fell more slowly (decay time constant, 20 ± 5 ms; 214 events analyzed in eight IHCs) (Fig. 1A). At −30 mV, somewhat larger and longer lasting outward currents were observed with an amplitude of 35 ± 9 pA, a time to peak of 19 ± 3 ms, and a decay time constant of 30 ± 4 ms (122 events analyzed in four IHCs). At intermediate voltages, the waveform was biphasic with an inward peak followed by a longer lasting outward current (Fig. 1B). The estimated reversal of the later outward current was around −80 mV, suggesting that this component was carried by potassium (equilibrium potential E_K at −82 mV).

We elevated extracellular potassium from 5.8 to 15 mM to depolarize synaptic terminals (Fig. 2A) (*5*). This caused a steady inward current in IHCs voltage-clamped to −80 mV (as expected from the resting potassium conductance with E_K now at −58 mV). In addition, both the frequency and amplitude of the spontaneous currents were increased by this change. The increased frequency is presumably due to increased transmitter release from depolarized efferent terminals. The increase in amplitude arose in part from the larger potassium driving force at −80 mV, but also possibly was affected by increased multiquantal release as well.

Given the probable synaptic origin of the spontaneous currents, we next examined their pharmacology. The biphasic waveform of the currents is reminiscent of ACh-evoked currents in hair cells of chicks and mammals (*6*). There, an early inward cation current flows through α9-containing ACh receptors. The Ca^{2+} influx through these channels then activates Ca^{2+}-dependent small-conductance (SK) potassium channels and thereby induces an outward current. Thus, we tested the ability of α-bungarotoxin (α-BTX) and strychnine, antagonists of the α9 receptor, to affect the spontaneous currents. Spontaneous inward currents were completely blocked by 300 nM α-BTX at −90 mV within 25 to 40 s (n = 3) (Fig. 2B). Although we could not demonstrate washout for α-BTX, the time course of the block was similar to that for the block of exogenously applied ACh (Fig. 3). Within 1 s, 1 μM strychnine completely blocked spontaneous currents (n = 4). Within 20 s, 100 nM strychnine blocked spontaneous currents, and currents were recovered after washout (n = 2) (Fig. 2C); in one experiment, block and recovery was induced twice. The SK channel blocker apamin reduced spontaneous currents in four IHCs within 15 and 45 s. Outward spontaneous currents at −30 mV were eliminated by 1 or 10 nM apamin in two IHCs (Fig. 2D). Inward currents at −90 mV were reduced in amplitude by 1 nM apamin in two IHCs. The residual current at −90 mV is presumed to flow through the ACh receptors, which are themselves cation channels and insensitive to apamin.

We next determined how IHCs respond to ACh. At −80 mV, 100 μM ACh caused inward currents in 53 of 55 IHCs with amplitudes between 20 and 400 pA (Fig. 3A).

The Center for Hearing Sciences, Department of Otolaryngology–Head and Neck Surgery, Johns Hopkins University School of Medicine, Baltimore, MD 21205, USA.

*To whom correspondence should be addressed. E-mail: eglowatz@bme.jhu.edu